

## Electron Transfer

Three-Way Cooperativity in  $d^8$  Metal Complexes with Ligands Displaying Chemical and Redox Non-InnocenceNaina Deibel,<sup>[a]</sup> Stephan Hohloch,<sup>[b]</sup> David Schweinfurth,<sup>[b]</sup> Fritz Weisser,<sup>[b]</sup> Anita Grupp,<sup>[a]</sup> and Biprajit Sarkar<sup>\*[b]</sup>

Dedicated to Prof. Konrad Seppelt on the occasion of his 70th birthday

**Abstract:** Reversible proton- and electron-transfer steps are crucial for various chemical transformations. The electron-reservoir behavior of redox non-innocent ligands and the proton-reservoir behavior of chemically non-innocent ligands can be cooperatively utilized for substrate bond activation. Although site-decoupled proton- and electron-transfer steps are often found in enzymatic systems, generating model metal complexes with these properties remains challenging. To tackle this issue, we present herein complexes  $[(\text{cod}_{-H})M(\mu-L^{2-})M(\text{cod}_{-H})]$  ( $M = \text{Pt}^{\text{II}}$ , [1] or  $\text{Pd}^{\text{II}}$ , [2],  $\text{cod} = 1,5$ -cyclooctadiene,  $\text{H}_2\text{L} = 2,5$ -di-[2,6-(diisopropyl)anilino]-1,4-benzoquinone), in which  $\text{cod}$  acts as a proton reservoir, and  $L^{2-}$  as an electron reservoir. Protonation of [2] leads to an un-

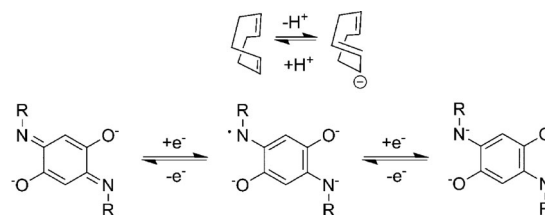
usual tetranuclear complex. However, [1] can be stepwise reversibly protonated with up to two protons on the  $\text{cod}_{-H}$  ligands, and the protonated forms can be stepwise reversibly reduced with up to two electrons on the  $L^{2-}$  ligand. The doubly protonated form of [1] is also shown to react with  $\text{OMe}^-$  leading to an activation of the  $\text{cod}$  ligands. The site-decoupled proton and electron reservoir sources work in tandem in a three-way cooperative process that results in the transfer of two electrons and two protons to a substrate leading to its double reduction and protonation. These results will possibly provide new insights into developing catalysts for multiple proton- and electron-transfer reactions by using metal complexes of non-innocent ligands.

## Introduction

Proton- and electron-transfer processes are elementary steps that are crucial for various bond-activation reactions used by enzymatic systems for substrate conversion.<sup>[1]</sup> For example, in cytochrome P450, protonated arginine and lysine act as proton sources, and nicotinamide adenine dinucleotide phosphate (NADPH) as an electron source to make the activation of  $\text{O}_2$  possible, which then eventually leads to C–H oxygenation reactions.<sup>[1b]</sup> Combining proton-transfer steps with electron-transfer steps has the obvious advantage of maintaining low reduction potentials for the electron-transfer processes. In enzymatic systems, the source of electrons and protons are usually different, and these centers cooperate at the active site to make substrate activation possible.<sup>[1]</sup> Redox non-innocent ligands are excellent tools for electron storage, and this property of such ligands has been recently utilized for performing catalytic bond-activation reactions.<sup>[2]</sup> On the other hand, chem-

ically non-innocent ligands are capable of acting as proton-storage sites, and this concept has been used for catalysis with metal complexes of pincer-type ligands.<sup>[3]</sup>

1,5-Cyclooctadiene ( $\text{cod}$ ) and its related counterparts can bind in a chelating  $\eta^2, \eta^2$  fashion to transition-metal centers and are known to be susceptible to deprotonation reactions in the metal-bound state. In doing so, the hapticity of such ligands changes from  $\eta^2, \eta^2$  to  $\eta^2, \eta^1$ , whereby deprotonation of  $\text{cod}$  leads to a change of one of the olefin donors to a carbanionic donor (Scheme 1).<sup>[4a–g]</sup> Coordination of the  $\eta^2, \eta^3$  ( $\pi$ -allyl) type is also known for the deprotonated form of  $\text{cod}$ .<sup>[4i–j]</sup> Ligands, such as 2,5-di-[2,6-(diisopropyl)anilino]-1,4-benzoquinone ( $\text{H}_2\text{L}$ ), on the other hand, are typical examples of redox non-innocent ligands.<sup>[2]</sup> Such ligands in their deprotonated and metal-coordinated form are capable of undergoing various reversible electron-transfer steps, and can thus exist in different



**Scheme 1.** Chemical non-innocence of  $\text{cod}$  (top) and redox non-innocence of diimino-quinone ligands (bottom).

[a] Dr. N. Deibel, Dr. A. Grupp  
Institut für Anorganische Chemie  
Universität Stuttgart, Pfaffenwaldring 55, 70569, Stuttgart (Germany)

[b] S. Hohloch, Dr. D. Schweinfurth, F. Weisser, Prof. Dr. B. Sarkar  
Institut für Chemie und Biochemie, Anorganische Chemie  
Freie Universität Berlin, Fabeckstrasse 34-36, 14195, Berlin (Germany)  
E-mail: biprajit.sarkar@fu-berlin.de

Supporting information for this article is available on the WWW under <http://dx.doi.org/10.1002/chem.201403276>. It contains experimental details.

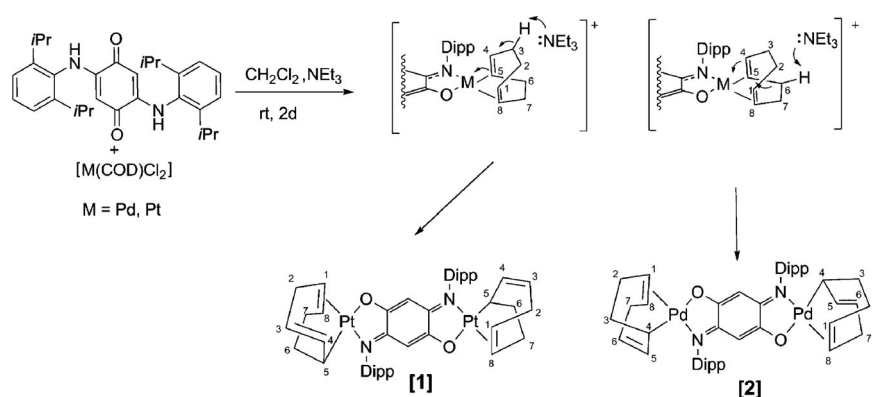
redox forms (Scheme 1).<sup>[5]</sup> Even though there have been some reports on transition-metal complexes that contain cod and a redox-active ligand,<sup>[6]</sup> to the best of our knowledge, reports on stepwise reversible proton- and electron-transfer studies in metal complexes combining these ligands remain rare.<sup>[6d–j]</sup>

We have been interested in various facets of metal complexes of redox-active ligands, including performing bond-activation reactions with them.<sup>[7]</sup> For generating such metal complexes, we have used redox non-innocent ligands that contain one or more [NR] groups because of the possibilities to tune the steric and electronic properties that the R groups offer in such ligands.<sup>[8]</sup> Herein, we present the metal complexes  $[(\text{cod}_{-H})M(\mu\text{-L}^{2-})M(\text{cod}_{-H})]$  ( $M = \text{Pt}^{\text{II}}$ , [1] or  $\text{Pd}^{\text{II}}$ , [2]), in which the deprotonated form of cod is bound to the metal centers. The protonation products of these complexes are reported. Furthermore, we show that in [1], reversible stepwise protonation/deprotonation of the cod ligands, and reversible reduction/oxidation of the  $\text{L}^{2-}$  ligands are possible. We finally show that these remote proton- and electron-transfer sites can work in tandem for performing substrate bond activation. Compounds [1] and [2], as well as all their various reduced and protonated forms, have been characterized by an arsenal of structural, electrochemical, and spectroelectrochemical methods.

## Results and Discussion

### Synthesis and characterization

The complexes [1] and [2] were synthesized by the reactions of  $[\text{Pt}(\text{cod})\text{Cl}_2]$  or  $[\text{Pd}(\text{cod})\text{Cl}_2]$ , respectively with  $\text{H}_2\text{L}$  in the presence of  $\text{NEt}_3$ .  $^1\text{H}$  NMR spectra of [1] and [2] indicated the loss of one proton each from the cod ligands, which was later confirmed by X-ray crystal structures of these complexes (see below). The deprotonation step likely proceeds through an initial coordination of cod ligand to the metal centers in the  $\eta^2, \eta^2$  mode through the olefinic double bonds, as was found in the precursor complex  $[\text{Pt}(\text{cod})\text{Cl}_2]$ . The coordinated cod is then deprotonated by  $\text{NEt}_3$  present in the reaction mixture (Scheme 2). This process leads to the generation of metal-coordinated  $\text{cod}_{-H}$  and a change in the coordination mode from



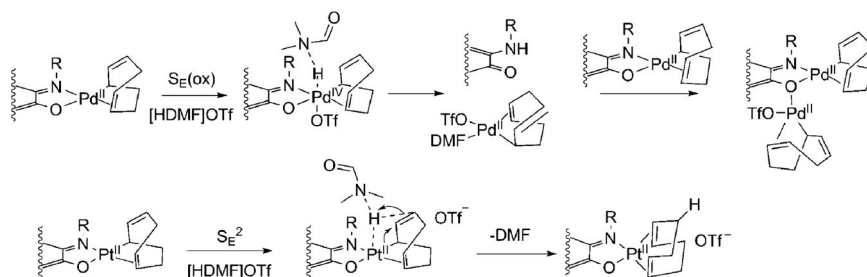
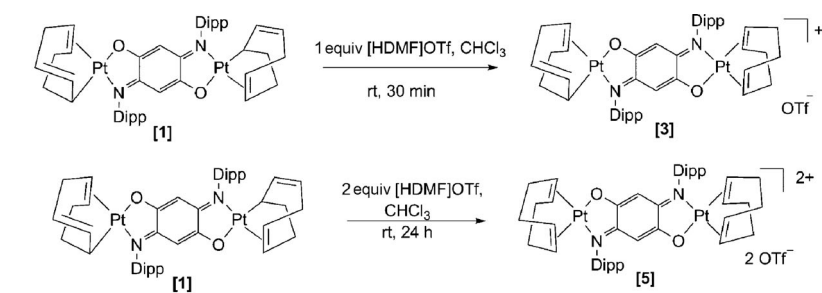
Scheme 2. Mechanism of formation of [1] and [2].<sup>[4d]</sup>

$\eta^2, \eta^2$  to  $\eta^2, \eta^1$ , with the formation of a 1,2- $\eta$ -6- $\sigma$ -cycloocta-1,4-dienyl (alkene/allyl) ligand.<sup>[4c–f]</sup> The eventual formation of a neutral species, which is less reactive, is a likely reason for this base-induced transformation. Remarkably, the position of deprotonation at the cod ligand is dependent on the metal center, as can be seen from a comparison of the X-ray crystal structures of [1] and [2] (Scheme 2).

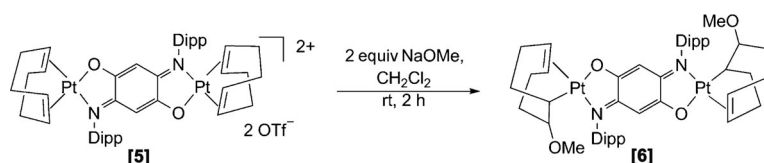
We were next interested in exploring if the  $\text{cod}_{-H}$  ligands in [1] and [2] can be protonated back to cod leading to the conversion of the allyl ligand to an olefin and a concomitant change in the hapticity of the ligands. Gratifyingly, the protonation of [1] with one equivalent of HDMF[OTf] ( $\text{DMF} = N,N$ -dimethylformamide,  $\text{OTf}^- = \text{triflate}$ ) led to a protonation of one of the  $\text{cod}_{-H}$  ligands leading to the formation of  $[(\text{cod}_{-H})\text{Pt}(\mu\text{-L}^{2-})\text{Pt}(\text{cod})](\text{OTf})$ , [3]. The formation of [3] and the change of one of the ligands from carbanionic to olefin were proven by NMR spectroscopy. Surprisingly, protonation of the palladium complex [2] with one equivalent of HDMF[OTf] led to the formation of an unusual tetranuclear complex, the structure of which was confirmed by single-crystal X-ray diffraction (see below). Based on literature reports,<sup>[9]</sup> we propose two different reaction pathways for the reaction of [1] and [2] with HDMF[OTf] (Scheme 3).

Protonation of [1] proceeds through a metal-assisted concerted protonation of  $\text{cod}_{-H}$ . This process leads to the release of DMF, and the change of allyl to alkene. However, for [2], the initial step is likely an oxidative addition to the  $\text{Pd}^{\text{II}}$  center, whereby  $\text{OTf}^-$  and  $\text{HDMF}^+$  are added to the palladium center. Reductive elimination leads to the release of the ligand  $\text{H}_2\text{L}$ .<sup>[9]</sup> The thus formed reactive complex containing a labile DMF ligand can react with unreacted [2] present in solution to generate the tetranuclear complex [4]. In compound [4], the O donors of  $\text{L}^{2-}$  act as a bridge between two  $\text{Pd}^{\text{II}}$  centers (Scheme 3). The detection of free  $\text{H}_2\text{L}$  during the protonation of [2], as well as the known propensity of palladium to readily undergo oxidative-addition and reductive-elimination reactions lend support to the proposed mechanism. The diplatinum complex [3] can be further protonated with another equivalent of HDMF[OTf] to generate  $[(\text{cod})\text{Pt}(\mu\text{-L}^{2-})\text{Pt}(\text{cod})](\text{OTf})_2$ , [5]. The cod ligands in [5] are all bound to the metal centers through olefinic double bonds (Scheme 3).

The doubly protonated complex [5] was reacted with NaOMe. This reaction leads to complex [6], in which the cod ligands have been activated by the formation of new C–OMe bonds through nucleophilic attack (Scheme 4). The addition of  $\text{OMe}^-$  to the cod ligands leads to a  $\pi/\sigma$  rearrangement and to the change in their hapticity from  $\eta^2, \eta^2$  to  $\eta^2, \eta^1$ . Such rearrangements are text-book examples of converting olefin complexes to alkyl complexes.<sup>[4a,b]</sup>



**Scheme 3.** Addition of protons to [1], and the corresponding coordination changes at the metal centers (top). Proposed reaction mechanism for the protonation reactions of [1] and [2] (bottom); only half of the molecule is shown for clarity with [2] on top and [1] at the bottom. Adapted from Reference [9].



**Scheme 4.** Reaction of [5] with NaOMe leading to the formation of [6].

All the complexes were characterized by NMR spectroscopy, elemental analysis, and mass spectrometry (see the Experimental Section in the Supporting Information). NMR spectroscopy already pointed to the different hapticity of the cod ligands in the various complexes. This fact was further confirmed by the single-crystal X-ray diffraction studies on the metal complexes.

### Crystal structures

Single crystals of the complexes [1], [2], [4], [5], and [6] suitable for diffraction studies were grown and used for X-ray diffraction studies (see the Experimental Section in the Supporting Information). Crystallographic details are listed in Table S1, and selected bond lengths and bond angles are given in Tables S2–S4 in the Supporting Information. The metal centers in all the complexes have a distorted square-planar coordination geometry (Figure 1). In compounds [1] and [2], each cod<sub>H</sub> ligand displays a  $\eta^2, \eta^1$  coordination. The distance between the C1C and C8C atoms (the additional “C” refers to atoms from the cod ligands) in [1] is 1.39(2) Å, and these two atoms of cod<sub>H</sub> are bound to the Pt<sup>II</sup> center in a  $\eta^2$  coordination mode. Additionally, the C3C–C4C bond length is 1.35(2) Å, and this bond forms the “allyl part” of the coordination together with the carbanionic C5C atom that is bound  $\eta^1$  to the Pt<sup>II</sup> center. As was expected, all other C–C bond lengths within

the cod<sub>H</sub> rings are longer than the two bond lengths mentioned above (Table S2 in the Supporting Information). The bond lengths within the Pd<sup>II</sup> analogue [2] are similar to [1], except that the position of the double bond neighboring the carbanionic donor is now at C5C–C6C. This is a consequence of the different positions of deprotonation of the cod ligands in [1] and [2], as has been discussed above. The metal–metal distances in both [1] and [2] are around 8 Å (Table S3 in the Supporting Information).

In the centrosymmetric tetranuclear Pd<sup>II</sup> complex [4], two of the Pd<sup>II</sup> centers are each bound to the O,N donors of the bridging L<sup>2-</sup> ligand, and to a  $\eta^2, \eta^1$ -coordinated cod<sub>H</sub> ligand (Figure 2). The other two Pd<sup>II</sup> centers are each bound to a triflate ligand and a cod<sub>H</sub> ligand with the fourth coordination site being occupied by an O donor of L<sup>2-</sup>, which bridges two Pd<sup>II</sup> centers. The bonding inside the cod<sub>H</sub> ligand is similar to the dinuclear complexes discussed

above. The distance between the O,N-coordinated Pd<sup>II</sup> centers is 8.1 Å. Additionally, the distances between the Pd<sup>II</sup> centers coordinated through the same O donor is 3.75 Å, and that between the two *anti* Pd<sup>II</sup> centers is 8.42 Å. Thus, as has been discussed above, protonation of the Pd<sup>II</sup> complex [2] results in this unusual tetranuclear complex [4].

Complex [5], which is the doubly protonated form of [1], is centrosymmetric. Additionally, [5] has a  $S_2$  axis running through the cod ligands and the central quinone ring (Figure 3). Both cod ligands in [5] are  $\eta^2, \eta^2$ -coordinated to the Pt<sup>II</sup> centers. Accordingly, the C1C–C1C bond lengths of 1.37 Å and the C4C–C4C bond lengths of 1.35 Å are the shortest distances within the cod rings (Table S2 in the Supporting Information). The Pt–Pt distance in [5] is 7.8 Å.

In complex [6], the activated cod ligands are bound to the Pt<sup>II</sup> centers in a  $\eta^2, \eta^1$  fashion (Figure 3). The C1C–C8C distance of 1.37 Å is the shortest C–C distance within the activated cod ligands (Table S2 in the Supporting Information). This data thus clearly points to alkene/alkyl coordination in complex [6] and the  $\pi/\sigma$  rearrangement induced by the addition of OMe<sup>-</sup> to the cod ligands. The C9C–O2C distance of 1.39 Å establishes the formation of C–OMe bonds at the cod ligands.

In complexes [1], [2], [4], and [6] that contain an activated cod ligand, the bond lengths between the metal centers and the carbanionic C donor of the cod rings are slightly shorter

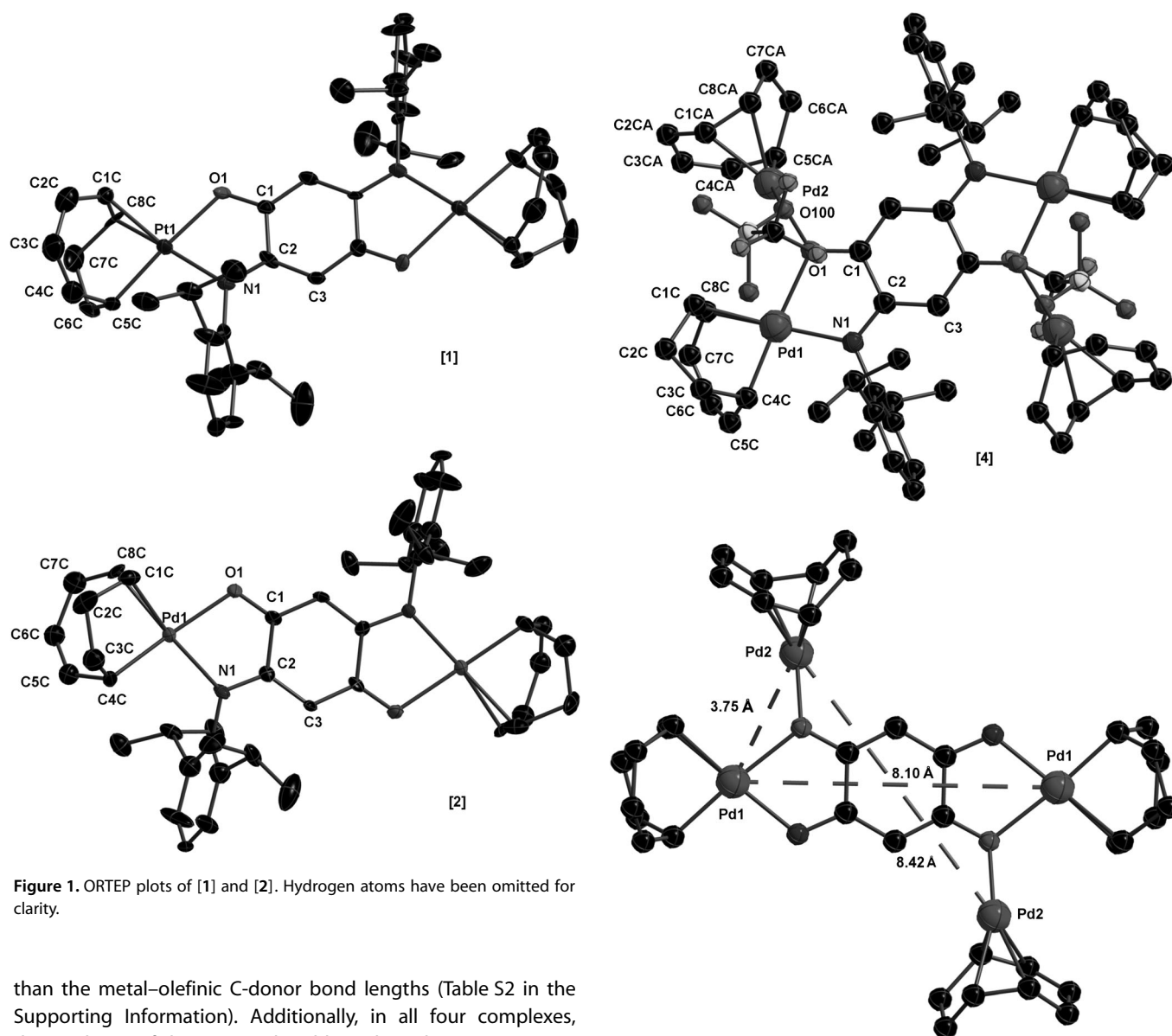


**Figure 1.** ORTEP plots of [1] and [2]. Hydrogen atoms have been omitted for clarity.

than the metal–olefinic C-donor bond lengths (Table S2 in the Supporting Information). Additionally, in all four complexes, the C<sup>-</sup> donor of the activated cod ligands is always *trans* to an O donor of the central bridging quinone ring (Figures 1–3). The stronger M–C(anionic) bond leads to a longer M–O (quinone) bond, possible due to its stronger *trans* influence when compared to a C=C bond.

A look at the bond lengths within the bridging quinone ligand ( $L^{2-}$ ) revealed C–O bond lengths that are closer to a single bond, and C=N bond lengths that are closer to a double bond (Table S2 in the Supporting Information). Accordingly, the neighboring C3–C1 (1.397 Å for [2]) bonds are shorter and the C2–C3 (1.430 Å) bonds are longer. These data point to the best description of  $L^{2-}$  as containing negatively charged O<sup>-</sup> and neutral imine type donors, with the negative charge being preferentially located on the more electronegative oxygen atoms.<sup>[8]</sup>

In all the complexes, the metal atoms and the central quinone ring are almost co-planar. The diisopropyl-phenyl substituents on the N atom of the quinone ring are perpendicular to the central quinone ring Figures 1–3.

**Figure 2.** Ball-and-stick plot of [4] (top). A perspective view of [4] showing the different Pd–Pd distances (bottom). Hydrogen atoms have been omitted for clarity.

### Cyclic voltammetry

The complexes [1]–[6] display a reversible one-electron reduction step. In addition, irreversible oxidation processes were observed for [1] and [2]. Furthermore, the complexes [1], [3], [5], and [6] showed a second one-electron reduction wave (Figures 4, S1 and S2 in the Supporting Information, and Table 1). By using THF as a solvent, which has a larger potential window on the negative side, the second reduction wave of [1] is more clearly visible (Figure S1 in the Supporting Information, top).

The redox potentials of the Pd<sup>II</sup> complex [2] are cathodically shifted compared to those of its Pt<sup>II</sup> analogue [1]. This probably leads to the expected second reduction for [2] falling outside the dichloromethane window (Table 1).

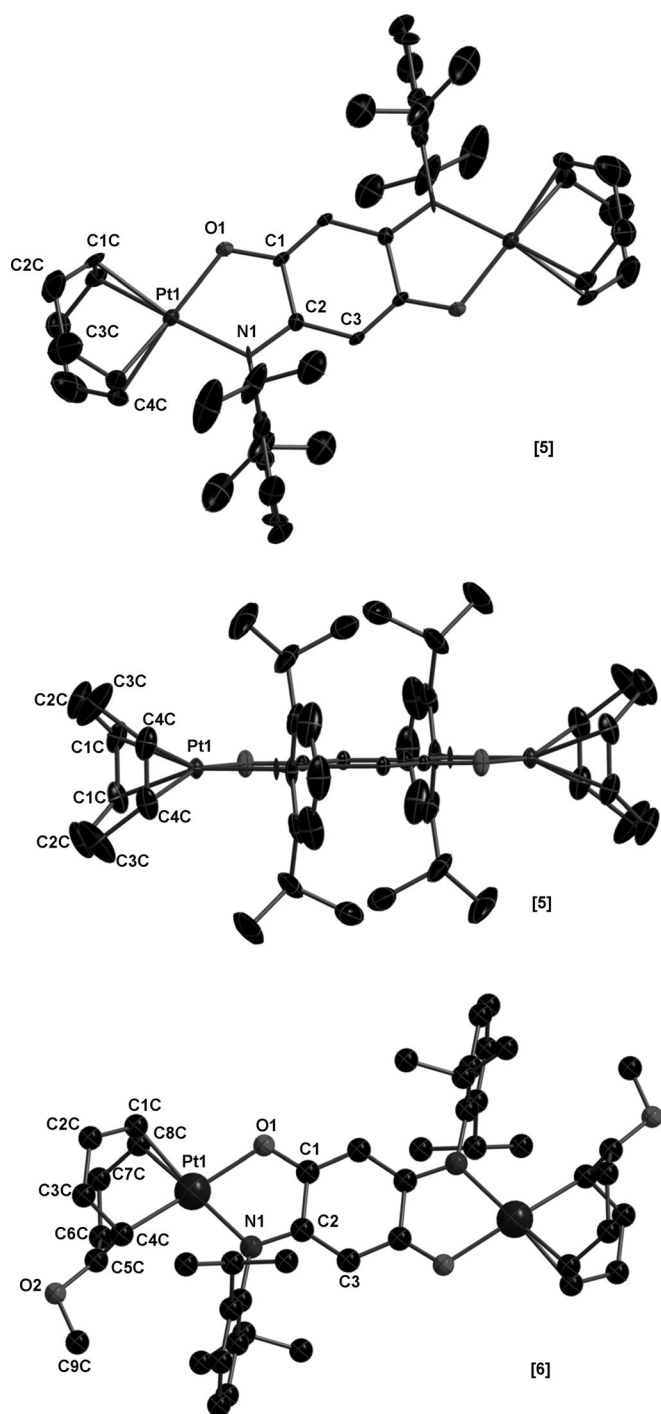


**Figure 3.** ORTEP plots of [5] (top). A perspective view of [5] to point out the center of inversion and the  $S_2$  axis (middle, see text for discussion). Ball-and-stick plot of [6] (bottom). Hydrogen atoms and counteranions are omitted for clarity.

Remarkably, complex [3], which is the mono-protonated form of [1], displayed two one-electron reduction steps, the potentials of which are anodically shifted by about 500 mV compared to [1]. Along the same lines, [5], which is the mono-protonated form of [3], displayed reduction potentials that are about 600 mV anodically shifted compared to [3] (Figure 4 and Table 1). Thus, the transfer of two protons to [1], which leads

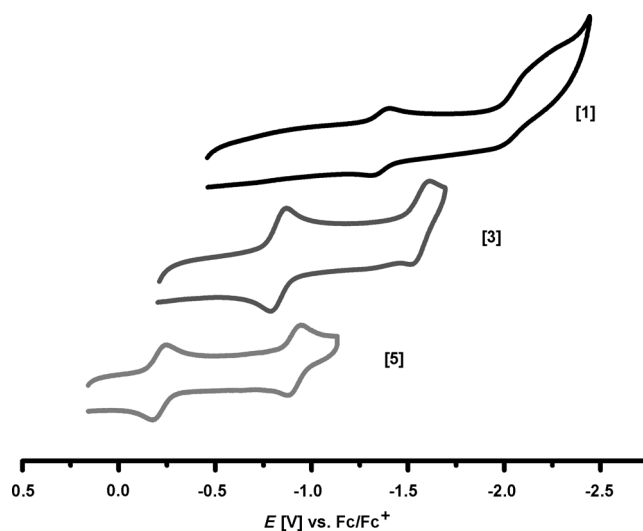


**Figure 4.** Cyclic voltammograms of [1], [3], and [5] in  $\text{CH}_2\text{Cl}_2/0.1 \text{ M Bu}_4\text{NPF}_6$  at 298 K. Scan rate:  $100 \text{ mV s}^{-1}$ . Ferrocene/ferrocenium was used as an internal standard.

Compound	$E^{\text{ox1}}$ [V]	$E^{\text{red1}}$ [V]	$E^{\text{red2}}$ [V]
[1]	0.70 <sup>[b]</sup>	-1.36	-2.09 <sup>[b]</sup>
[2]	0.61 <sup>[b]</sup>	-1.69	-
[3]	-	-0.83	-1.57
[4]	-	-1.95 <sup>[c]</sup>	-
[5]	-	-0.21	-0.91
[6]	-	-1.29	-1.98

[a] Half-wave potentials from cyclic voltammetric measurements in  $\text{CH}_2\text{Cl}_2/0.1 \text{ M Bu}_4\text{NPF}_6$  for reversible processes at 298 K, scan rate  $100 \text{ mV s}^{-1}$ ; ferrocene/ferrocenium was used as an internal standard. [b]  $E_{\text{pa}}$  for irreversible process. [c] At  $-40^\circ\text{C}$ .

to the formation of [5], makes the reduction potentials of [5] more than 1 V more facile compared to [1]. The increase in positive charge of the complexes on protonation is responsible for this huge shift in the redox potentials of the complexes. Complex [6], which contains cod rings with the OMe groups has redox potentials that are comparable to [1] (Figure S2 in the Supporting Information, Table 1). Thus, the addition of a OMe<sup>-</sup> group to cod seems to have the same influence on the redox potentials of the complex as the deprotonation of cod. This is probably so, because an anionic ligand is generated in each case.

The tetranuclear Pd<sup>II</sup> complex [4] displays a single redox event at  $-1.95 \text{ V}$ , which is chemically reversible only at low temperatures. The lower reversibility of this redox wave is likely associated with the bridging mode of the O atoms of  $\text{L}^{2-}$  in [4] (Figure 2). Such a fragile coordination is expected to break-up on changing the redox state of the complex, possibly leading to a lower reversibility of the redox process. The reduction potential for [4] is cathodically shifted by about 600 mV compared to the dinuclear Pd<sup>II</sup> complex [2].

To shed more light on the redox processes discussed above, spectroelectrochemical measurements and DFT calculations were carried out on the complexes.

### EPR, UV/Vis/NIR spectroelectrochemistry, and spin-density calculations

The one-electron reduced forms of complexes [1]–[6] were investigated by X-band EPR spectroscopy. The reduced complexes display similar spectra in fluid solutions with signals centered around  $g=2.0$  (Figure 5, Table 2). The spectra of the reduced forms of complexes [1], [2], and [4]–[6] were simulated by considering a hyperfine coupling of about 3–4 G to two equivalent  $^{14}\text{N}$  nuclei. Additionally, satellites to two equivalent

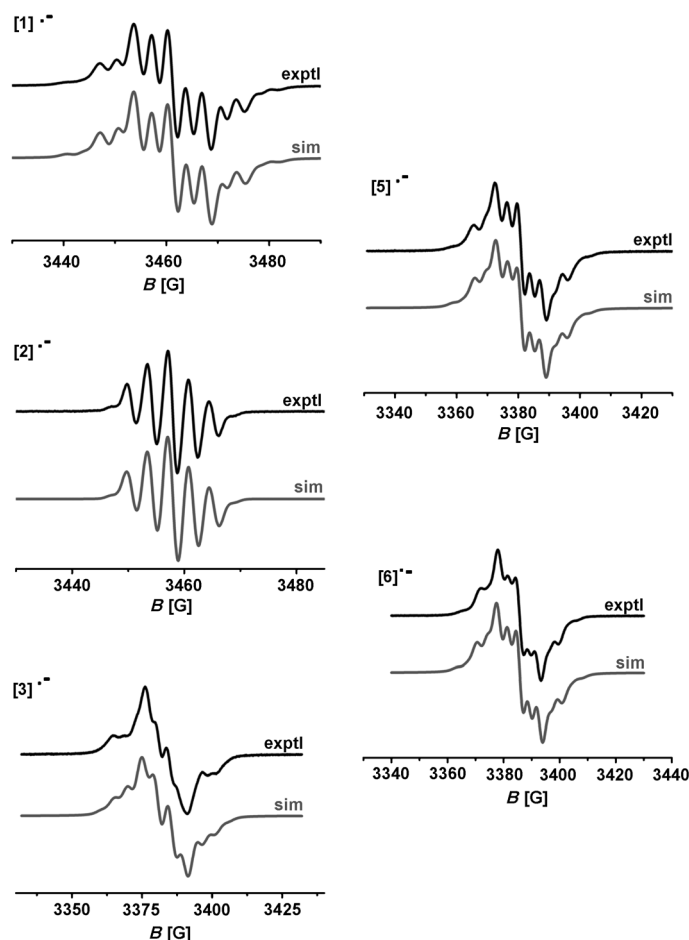


**Figure 5.** X-band EPR spectra of the mono-reduced forms of the complexes at 298 K. The anion-radical sign signifies the reduced state of the complexes and not the real charge.

$^{105}\text{Pd}$  or  $^{195}\text{Pt}$  nuclei were also considered in the simulations (Table 2). Remarkably, for the reduced state of the mono-protonated  $\text{Pt}^{\text{II}}$  complex [3], an asymmetric spin distribution was observed with hyperfine coupling to two inequivalent  $^{14}\text{N}$  nuclei of 4.5 and 2.2 G, respectively. Accordingly, the  $^{195}\text{Pt}$  coupling for this complex was also found to be different for the two Pt nuclei with values of 20 and 9.7 G. Thus, the inequivalence of the two cod rings in [3] seems to have an influence

Table 2. EPR data of the one-electron-reduced complexes. <sup>[a]</sup>			
Compounds	$g_{\text{iso}}$	$a_{\text{iso}} (^{14}\text{N})^{\text{[b]}}$	$a_{\text{iso}} (\text{M})^{\text{[b]}}$
[1] <sup>•-</sup>	1.999	$2 \times 3.15$	$2 \times 13.2^{\text{[c]}}$
[2] <sup>•-</sup>	2.002	$2 \times 3.65$	$2 \times 1.2^{\text{[d]}}$
[3] <sup>•-</sup>	1.999	4.5; 2.2	20.0; 9.7 <sup>[c]</sup>
[4] <sup>•-</sup>	2.002	$2 \times 3.9$	$2 \times 1.1^{\text{[d]}}$
[5] <sup>•-</sup>	1.999	$2 \times 3.3$	$2 \times 14.3^{\text{[c]}}$
[6] <sup>•-</sup>	1.999	$2 \times 3.3$	$2 \times 14.4^{\text{[c]}}$

[a] X-band EPR data obtained from in situ generated species in  $\text{CH}_2\text{Cl}_2/0.1 \text{ M Bu}_4\text{NPF}_6$  at 298 K, for  $4^{\text{-}}$  at 275 K. The anion-radical sign signifies the one-electron-reduced state of the complexes and not the total charge. [b] Isotropic hyperfine coupling constants in Gauss obtained from simulation. [c] Hyperfine coupling to  $^{195}\text{Pt}$ ,  $l=1/2$ , natural abundance = 33.3%. [d] Hyperfine coupling to  $^{105}\text{Pd}$ ,  $l=5/2$ , natural abundance = 22.2%.

on the spin-density distribution of the one-electron reduced form of that complex.

To shed further light on the EPR results, spin-density calculations were carried out for the one-electron reduced forms of selected complexes. Structural optimizations were carried out by using DFT method with the BP86 functional. A look at the Löwdin spin-density plot shows the spin density to be predominantly localized on the bridging ligand (Figure 6). For example, for the one-electron reduced form of [1], the two platinum centers combined contain a total spin density of only 3.2%, whereas 83% of the spin density is localized on the central bridging ligand. The two central carbon atoms of the bridge (and accordingly the protons attached to them) contain negligible spin density. The nitrogen atoms of the bridging ligand contain a total spin density of 29.2%. Despite this high spin density on the nitrogen atoms (compared to the platinum centers), the experimental hyperfine coupling observed for  $^{195}\text{Pt}$  is larger than that of  $^{14}\text{N}$  owing to the larger value of the intrinsic isotropic hyperfine coupling constant for  $^{195}\text{Pt}$  as compared to  $^{14}\text{N}$ . Similar results from spin-density calculations were obtained for the one-electron reduced forms of [2] and [5] (Figure S3 in the Supporting Information). For the one-electron reduced form of [3], which contains one cod and one cod<sub>H</sub> ligands, the spin-density distribution was found to be non-symmetrical (Figure S4 in the Supporting Information). For that species, one of the nitrogen atoms contain about 9.5% spin density, and the other contains about 20% spin density. A similar non-symmetrical spin-density distribution is also seen for the platinum centers for that compound. Thus, the spin-density calculations nicely corroborate the experimental EPR results.

The observation of the EPR signals for the one-electron reduced complexes in fluid solutions at ambient temperature (except for the reduced form of [4], in which the lower degree of chemical reversibility forced us to record a spectrum at 275 K), the  $g$  value close to 2.0, the hyperfine couplings observed to the two  $^{14}\text{N}$  nuclei of the  $\text{L}^{2-}$  ligand, and the results

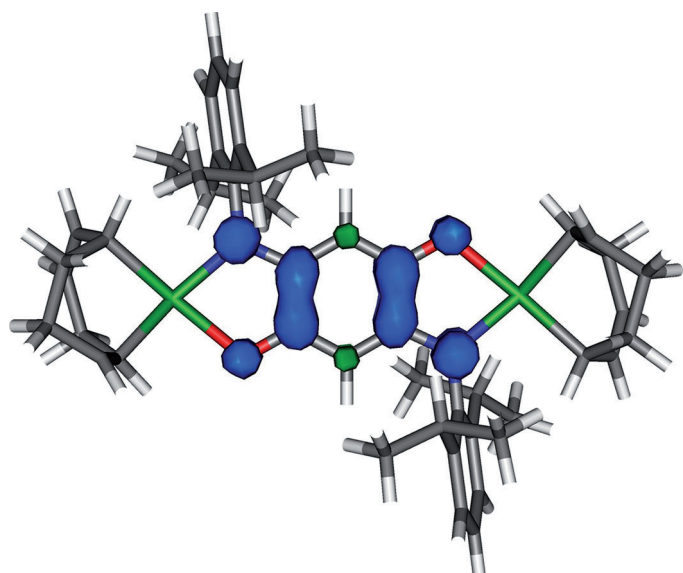


**Figure 6.** Lwdin spin-density plot for the one-electron reduced form of [1]. See text for explanation.

from spin-density calculations are clear indications of the reduction predominantly taking place on the bridging quinone ligand in all the investigated complexes.<sup>[8c,f]</sup> X-ray crystallographic and NMR studies (see below) have clearly established the cod ligand as the proton-transfer site. The EPR studies deliver compelling evidence for the quinone bridge  $L^{2-}$  being the electron-transfer site. Hence, the protonation of a remote cod ligand drastically influences the redox potentials (see electrochemistry section above) of the complexes for electron-transfer steps that occur on the bridging quinone ligand.

All investigated complexes display a main broad absorption band in the visible region (Figures 7, S5, and Table S5 in the Supporting Information), which is assigned to a mixture between an intra-ligand transition within the  $L^{2-}$  bridge, and a metal-to-ligand charge transfer (MLCT) transition from  $Pt^{II}$  to  $L^{2-}$ . It should be noted that ligands, such as  $H_2L$ , indeed display an absorption band in the visible region, which is responsible for their characteristic red color.<sup>[8]</sup>

The  $Pd^{II}$  complex [2] exhibits an absorption band at  $\lambda = 420$  nm, which appears at a higher energy compared to its  $Pt^{II}$  counterpart [1], for which this band appears at about 470 nm. As can be seen from Table 1, the difference between the oxidation and reduction potentials for [2] is larger than that for [1], and this fact seems to get reflected in the long wavelength bands of the complexes. Stepwise protonation of [1] to form [3] and [5] leads to a shift of the band in the visible region to higher energies; additional weak band at longer wavelengths were observed for [3] and [5] (Table S5 in the Supporting Information). The absorption band for complex [6] in the visible region appeared at 475 nm, which is comparable to the band observed for [1]. The tetranuclear  $Pd^{II}$  complex [4] displayed an absorption spectrum in the visible region, which is almost identical to its dinuclear counterpart [2] (Figure S5 and Table S5 in the Supporting Information).

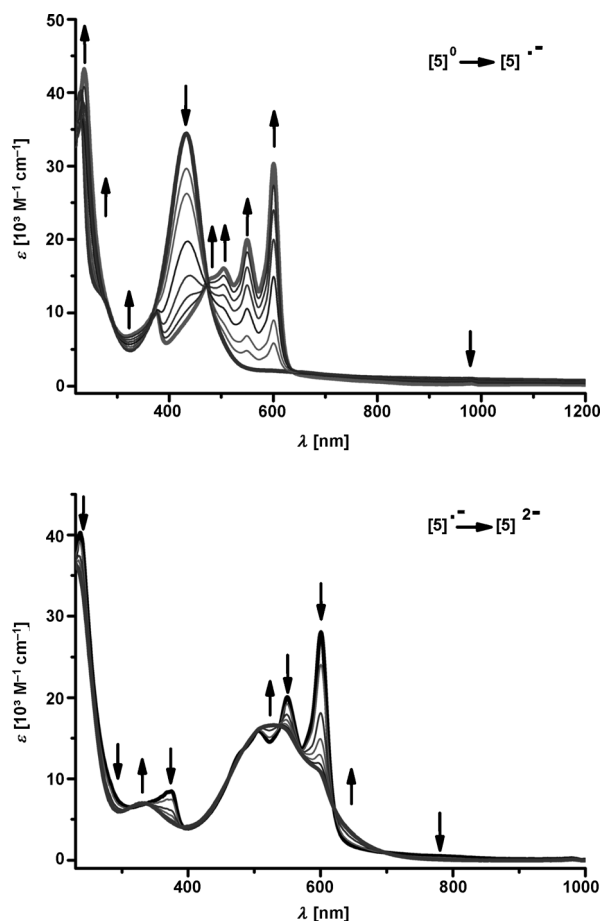


**Figure 7.** Changes in the UV/Vis/NIR spectrum of [5] during spectroelectrochemistry in an OTTE cell<sup>[10]</sup> in  $CH_2Cl_2/0.1$  M  $Bu_4NPF_6$ .

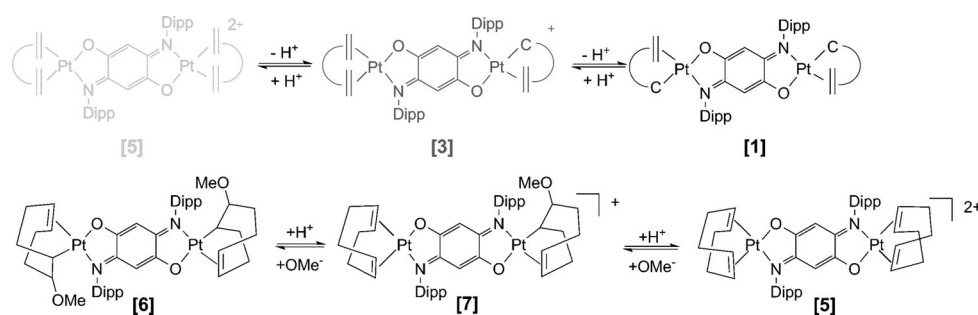
One-electron reduction of the complexes leads to a loss of intensity of the initial band in the visible region. New structured bands were observed at lower energies for the one-electron reduced states of all the complexes (Figures 7, S5, and Table S5 in the Supporting Information). These bands are assigned to a mixture of ligand-to-metal charge transfer (LMCT) transitions and transitions within the radical ligand  $L^{3-}$  formed on one-electron reduction of the complexes. Such structured bands in the visible region are typical for radicals of bridging ligands, such as the one described herein (free, as well as metal-bound, ones).<sup>[8]</sup> It was possible to obtain the spectroscopic signatures of the one- and two-electron reduced forms of the protonated diplatinum complexes [3] and [5]. In both cases, reduction by a further electron leads to a loss of the structured bands, and the appearance of a broad band (Figures 7, S5, and Table S3 in the Supporting Information). This band is assigned to an LMCT transition from a  $L^{4-}$  aromatic bridging ligand to the  $Pt^{II}$  centers. The bands in the UV region do not show much variation for the different complexes in their various oxidation states.

Thus, the spectroelectrochemistry measurements deliver the spectroscopic signatures for all the complexes in the various protonated and redox forms. This information will be used in

the following to elucidate reactivity studies with these metal complexes.

### Reactivity studies on and with the complexes

Pd<sup>II</sup> complex [2] leads to the formation of a tetranuclear complex on protonation (see above). We first attempted to check the reversibility of the protonation steps that lead to the conversion of [1] through [3] to [5]. UV/Vis spectroscopy was used to investigate this phenomenon, because the spectroscopic signatures of all the forms are known. Gratifyingly, the reaction of [5], which has an intense absorption band at  $\lambda=433$  nm, with NEt<sub>3</sub>, leads to stepwise changes in its UV/Vis spectrum leading first to the formation of a species, UV/Vis spectrum of which is identical to that of [3]. Further addition of NEt<sub>3</sub> generates a spectrum with an intense band at  $\lambda=470$  nm, which matches exactly the spectrum of [1] (Figure S6 in the Supporting Information). Deprotonation/protonation is also associated with color changes that can be followed with the naked eye. Thus, compound [5], which is green, first changes its color to brown green when one proton is removed to form [3], further deprotonation of [3] generates complex [1], which is brown (Scheme 5). Complex [1] can, of course, be protonated back



**Scheme 5.** Reactions with H<sup>+</sup> and OMe<sup>-</sup> for the diplatinum complexes. Double bonds are shown in the top Scheme to point to the generality of this process (not necessarily restricted to cod).

via [3] to [5], as has been discussed above. These reversible protonation/deprotonation reactions are associated with the change in the coordination mode of cod, which binds as an alkene/alkene ligand in the neutral state, and as a carbanion/alkene ligand in the negative cod<sub>-H</sub> form.

The complex [6] that contains methoxy-activated cod rings can also be protonated back to [5] via [7] by using [HDMF]-(OTf) (Scheme 5). The protonation reactions in this case have also been followed by UV/Vis spectroscopy. Thus, the band at  $\lambda=474$  nm for [6] first changes to an intermediate position before eventually shifting to 433 nm, which is the main absorption band in the visible region for [5] (Figure S7 in the Supporting Information). Even though we have not characterized the intermediate species [7] for this transformation by any other method, the stepwise changes in the UV/Vis spectrum coupled with the clean formation of [5] on double protonation make us believe that [7] was indeed formed during this protonation reaction. Compound [5] can be converted back to [6] by reacting it with NaOMe, as has been discussed above. Thus,

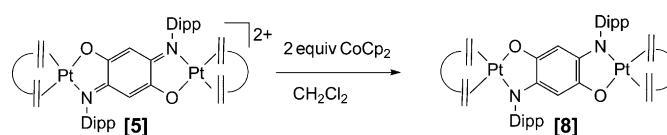
it is seen that the cod ligand can be reversibly activated by forming a C–OMe bond, which can then be reversible broken with a proton source. This conversion is associated with the coordination change of the cod ligands from an alkene/alkene form to an alkyl/alkene form. Recently, such a conversion has been reported for a mononuclear Pt<sup>II</sup> complex by making use of electron transfer from a redox-active ligand.<sup>[6a]</sup> We have shown herein an example, in which such a transformation can be performed through protonation. In both cases, it is the change in the total charge of the complex that probably makes such transformations possible. The reactions shown in Scheme 5 thus clearly prove the chemical non-innocence of the cod ligands in the complexes presented herein.<sup>[4h–j]</sup>

Compound [8], which is a highly air-sensitive compound, was characterized by NMR spectroscopy (Figure S8 in the Supporting Information) and UV/Vis spectroscopy. The UV/Vis spectrum of this chemically isolated species is identical to that observed during the in situ two-electron reduction of [5] observed during spectroelectrochemical measurements. To the best of our knowledge, [8] is the first example of a chemically isolated complex that has a tetra-reduced form of a quinone-derived ligand containing a [O,N,O,N] donor set. Even though such aromatic bridges have been stabilized in metal complexes

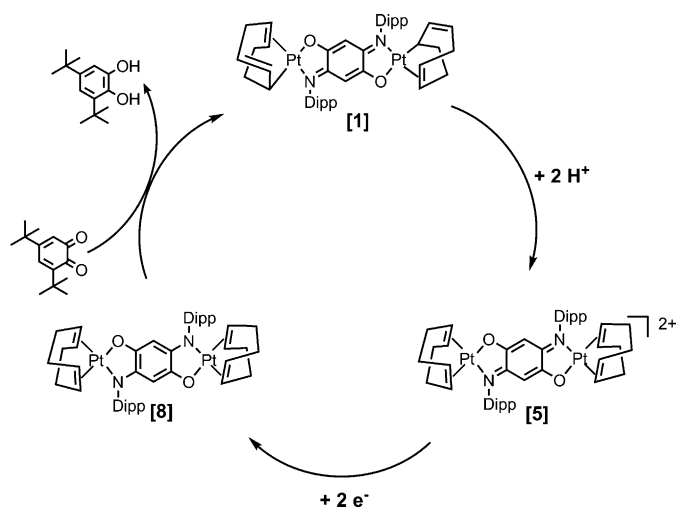
for quinone ligands containing a [O,O,O,O] donor set,<sup>[5g]</sup> it is usually difficult to stabilize corresponding aromatic systems that contain one or more NR donors because of the higher negative reduction potentials of such compounds. Remarkably, in the present case, it is the protonation of the remote cod ligand that helps in shifting the reduction potentials in the positive direction, and makes the isolation of compound [8] possible. Together with the spectroelectro-

chemical results the conversion of [5] to [8] establishes the redox non-innocent nature of L<sup>2-</sup> in these complexes.

Having unequivocally established the stepwise, reversible protonation steps for the cod ligands (Scheme 5) and the reversible electron-transfer steps for the L<sup>2-</sup> ligand (Scheme 6) in the investigated complexes, we were next interested in probing if these site-decoupled protons and electrons can be transferred in a three-way cooperative process to a substrate. After taking redox potentials into consideration, 3,5-di-*tert*-butylbenzoquinone was chosen as a substrate and its conversion to



**Scheme 6.** Chemical reduction of complex [5].



**Scheme 7.** Reaction cycle displaying transfer of two protons and two electrons to a substrate.

3,5-di-*tert*-butyl-catechol was probed by using [8] as an electron and proton source (Scheme 7).

To perform this reaction, [5] was reduced in situ with cobaltocene to [8], and the conversion was followed by UV/Vis spectroscopy. This conversion led to a color change from green to violet. Once [8] was formed, the substrate 3,5-di-*tert*-butyl-benzoquinone was added to the reaction mixture, which led to an immediate color change to orange. The UV/Vis spectrum of the mixture changed accordingly (Figure S9 in the Supporting Information). After stirring for 24 h, the reaction mixture was worked up (see the Experimental Section in the Supporting Information), and the isolated solid was subjected to NMR spectroscopy. The NMR spectrum of the isolated solid in  $CD_2Cl_2$  showed signals that correspond to [1], 3,5-di-*tert*-butyl-catechol and cobaltocenium (Figure S10 in the Supporting Information). Thus, compound [8] transfers two electrons and two protons to 3,5-di-*tert*-butyl-benzoquinone leading to its conversion to the catechol form. In the process, [8] gets converted to [1]. The cobaltocenium signal observed in the NMR spectrum arises from the oxidized form of cobaltocene, which is used for the in situ reduction of [5] to [8]. The isolated compound also displays a UV/Vis spectrum that matches with the main transition of [1] (Figure S9 in the Supporting Information). Compound [1] can now be protonated to convert it to [5], which closes the cycle (Scheme 7).

Thus, it is seen that two protons, one each from a different cod ligand, and two electrons from the bridging quinone ligand in [8] can be transferred to a substrate leading to its double protonation and double reduction. It is intriguing that such site-decoupled proton and electron sources can work in tandem to transfer electrons and protons to a particular substrate in a three-way cooperative process.

## Conclusion

We have presented herein diplatinum and dipalladium complexes that contain anionic  $cod_{-H}$  stopper ligands and a redox-active quinonoid bridging ligand. Protonation of the dipalladi-

um complex resulted in the generation of an unusual tetranuclear palladium complex, in which the  $cod_{-H}$  ligand retains its charge and coordination mode. On the other hand, the diplatinum complex can be reversibly protonated at the  $cod_{-H}$  ligands, whereby those ligands undergo a  $\sigma/\pi$  rearrangement and change their coordination mode from an allyl/alkene to an alkene/alkene mode. Additionally, we have shown that the  $cod$  ligands can also be activated by reaction of the protonated diplatinum complex with NaOMe through nucleophilic attack, which leads to the formation of a new C–OMe bond at the  $cod$  ligands and a change in their coordination mode from alkene/alkene to alkyl/alkene. For the diplatinum complexes, all protonation reactions, as well as the reaction with  $OMe^-$ , have been shown to be completely reversible. Reversible electron transfers have been observed at the bridging quinone ligands for all the complexes. The locus of the electron-transfer steps at the bridging quinone ligands has been unequivocally established by using UV/Vis and EPR spectroelectrochemical methods. We have also shown that the protonation of the remote  $cod_{-H}$  ligands leads to a shift of the bridging quinonoid ligand reduction by  $\geq 500$  mV/proton. Thus, the protonated complex displays reduction potentials that are more than one Volt positively shifted compared to its non-protonated counterpart. Taking advantage of this low reduction potential, we have managed to chemically isolate the first example of a dinuclear complex containing an aromatic bridge of a quinone-derived ligand with a [O,N,O,N] donor set. The doubly protonated and doubly reduced diplatinum complex has been utilized in a three-way cooperative process to transfer two protons from two different  $cod$  ligands and two electrons from the bridging quinone ligand to reduce 3,5-di-*tert*-butyl-benzoquinone to 3,5-di-*tert*-butyl-catechol (Scheme 7). The protonation at the remote  $cod$  ligands helps to control reduction potentials of electron-transfer steps occurring at the site-decoupled quinone bridge. It is the achievement of low reduction potentials that finally makes electron and proton transfer to the substrate possible.

Control of redox potentials through remote protonation steps is common in biological systems, and biocatalysis usually works through transfer of electrons and protons. Most man-made homogeneous catalysts on the other hand take advantage of oxidative addition and reductive elimination steps for substrate activation and transformation. However, in recent years, examples of substrate activation by consecutive proton- and electron-transfer steps have appeared with man-made catalysts.<sup>[2c]</sup> We believe that the proof of concept that we have delivered in this work of site decoupled proton and electron transfer sites that can work in tandem for performing substrate bond activation will further contribute to develop concepts for new kinds of catalysis. Additionally, we have also shown that spectroelectrochemistry is a powerful technique to determine spectroscopic signatures of reactive intermediates that appear in bond-activation processes. These spectroscopic signatures can then be utilized to elucidate the pathway of substrate activation in such complexes containing non-innocent ligands. We note that all proton- and electron-transfer steps observed in these complexes are ligand based.

## Acknowledgements

Carl-Zeiss Stiftung is kindly acknowledged for financial support of this project (docortal stipend for N.D.). We thank Alexa Paratzki for the initial synthesis and characterization of complexes [1] and [2]. Dr. Fabian Ehret is acknowledged for EPR measurements, and Prof. Dr. D. Lentz for crystallographic measurements of [1] and [2]. We are grateful to ZEDAT, FU Berlin for access to the computing facilities.

**Keywords:** bond activation • electron transfer • ligand effects • quinones • spectroelectrochemistry

- [1] a) W. Kaim, B. Schwederski, A. Klein, *Bioinorganic Chemistry: Inorganic Elements in the Chemistry of Life: An Introduction and Guide*, 2nd ed. John Wiley & Sons, Chichester, **2013**; b) B. Meunier, S. P. de Visser, S. Shaik, *Chem. Rev.* **2004**, *104*, 3947.
- [2] For selected examples, see: a) P. Chaudhuri, C. N. Verani, E. Bill, E. Bothe, T. Weyhermüller, K. Wieghardt, *J. Am. Chem. Soc.* **2001**, *123*, 2213; b) E. Bill, E. Bothe, P. Chaudhuri, K. Chlopek, D. Herebian, S. Kokatam, K. Ray, T. Weyhermüller, F. Neese, K. Wieghardt, *Chem. Eur. J.* **2005**, *11*, 204; c) R. E. Rodríguez-Lugo, M. Trincado, M. Vogt, F. Tewes, G. Santiso-Quinones, H. Grützmacher, *Nat. Chem.* **2013**, *5*, 342; d) B. de Bruin, D. G. H. Hetterscheid, A. J. J. Koekkoek, H. Grützmacher, *Prog. Inorg. Chem.* **2007**, *55*, 247; e) P. J. Chirik, K. Wieghardt, *Science* **2010**, *327*, 794; f) M. R. Ringenberg, S. L. Kokatam, Z. M. Heiden, T. B. Rauchfuss, *J. Am. Chem. Soc.* **2008**, *130*, 788; g) V. K. K. Praneeth, M. R. Ringenberg, T. R. Ward, *Angew. Chem.* **2012**, *124*, 10374; h) W. I. Dzik, J. I. van der Vlugt, J. N. H. Reek, B. de Bruin, *Angew. Chem.* **2011**, *123*, 3416; i) A. I. Nguyen, K. J. Blackmore, S. M. Carter, R. A. Zarkesh, A. F. Heyduk, *J. Am. Chem. Soc.* **2009**, *131*, 3307; j) M. K. Tsai, J. Rochford, D. E. Polyansky, T. Wada, K. Tanaka, J. T. Muckerman, *Inorg. Chem.* **2009**, *48*, 4372; k) Forum Issue on Redox-Active Ligands, *Inorg. Chem.* **2011**, *50*, 9737–9914; l) Cluster Issue, Cooperative and Redox Non-Innocent Ligands in Directing Organometallic Reactivity, *Eur. J. Inorg. Chem.* **2012**, 340–580; m) O. R. Luca, R. H. Crabtree, *Chem. Soc. Rev.* **2013**, *42*, 1440; n) A. M. Tondreau, C. C. H. Atienza, K. J. Weller, S. A. Nye, K. M. Lewis, J. G. P. Delis, P. J. Chirik, *Science* **2012**, *335*, 567; o) V. Lyaskovskyy, B. de Bruin, *ACS Catal.* **2012**, *2*, 270.
- [3] For selected examples see: a) J. Zhang, G. Leitus, Y. Ben-David, D. Milstein, *J. Am. Chem. Soc.* **2005**, *127*, 10840; b) C. Gunanathan, Y. Ben-David, D. Milstein, *Science* **2007**, *317*, 790; c) J. Schöffel, A. Y. Rogachev, S. De Beer George, P. Burger, *Angew. Chem. Int. Ed.* **2009**, *48*, 4734; *Angew. Chem.* **2009**, *121*, 4828; d) D. Sieh, P. Burger, *J. Am. Chem. Soc.* **2013**, *135*, 3971; e) E. Ben-Ari, G. Leitus, L. J. W. Shimon, D. Milstein, *J. Am. Chem. Soc.* **2006**, *128*, 15390.
- [4] a) R. H. Crabtree, *The Organometallic Chemistry of Transition Metals*, 5th ed. John Wiley & Sons, Hoboken, **2009**; b) C. Elschenbroich, *Organometallics*, 3rd ed. Wiley-VCH, Weinheim, **2006**; c) A. M. Gull, P. E. Fanwick, C. P. Kubiak, *Organometallics* **1993**, *12*, 2121; d) J. C. Peters, S. B. Harkins, S. D. Brown, M. W. Day, *Inorg. Chem.* **2001**, *40*, 5083; e) R. Mas-Ballesté, P. A. Champkin, W. Clegg, P. Gonzalez-Duarte, A. Lledos, G. Ujaque, *Organometallics* **2004**, *23*, 2522; f) W. Petz, C. Kutschera, B. Neumüller, *Organometallics* **2005**, *24*, 5038; g) D. Aguilar, F. Aznarez, R. Bielsa, L. R. Falvello, R. Navarro, E. P. Urriolabeitia, *Organometallics* **2007**, *26*, 6397; h) A. J. C. Walters, O. Troepner, I. Ivanovic-Burmazovic, C. Tejel, M. P. del Rio, J. N. H. Reek, B. de Bruin, *Angew. Chem. Int. Ed.* **2012**, *51*, 5157; *Angew. Chem.* **2012**, *124*, 5247; i) D. G. H. Hetterscheid, M. Klop, R. J. N. A. M. Kicken, J. M. M. Smits, E. J. Reijerse, B. de Bruin, *Chem. Eur. J.* **2007**, *13*, 3386; j) D. G. H. Hetterscheid, B. de Bruin, J. M. M. Smits, A. W. Gal, *Organometallics* **2003**, *22*, 3022.
- [5] For selected examples see: a) M. D. Ward, *Inorg. Chem.* **1996**, *35*, 1712; b) M. Leschke, M. Melter, H. Lang, *Inorg. Chim. Acta* **2003**, *350*, 114; c) S. Kitagawa, S. Kawata, *Coord. Chem. Rev.* **2002**, *224*, 11; d) C. Carbonera, A. Dei, J.-F. Letard, C. Sangregorio, L. Sorace, *Angew. Chem. Int. Ed.* **2004**, *43*, 3136; *Angew. Chem.* **2004**, *116*, 3198; e) J. S. Miller, K. S. Min, *Angew. Chem. Int. Ed.* **2009**, *48*, 262; *Angew. Chem.* **2009**, *121*, 268; f) B. Therrien, G. Süß-Fink, P. Govindaswamy, A. K. Renfrew, P. J. Dyson, *Angew. Chem.* **2008**, *120*, 3833; g) K. Heinze, G. Huttner, O. Walter, *Eur. J. Inorg. Chem.* **1999**, 593; h) Y.-F. Han, W.-G. Jia, W.-B. Yu, G.-X. Jin, *Chem. Soc. Rev.* **2009**, *38*, 3419; i) Y.-F. Han, H. Li, G.-X. Jin, *Chem. Commun.* **2010**, 46, 6879; j) H. Jung, A. Dubey, H. J. Koo, V. Vajpayee, T. R. Cook, H. Kim, S. C. Kang, P. J. Stang, K.-W. Chi, *Chem. Eur. J.* **2013**, *19*, 6709; k) T. E. Keyer, R. J. Forster, P. M. Jayaweera, C. G. Coates, J. J. McGarvey, J. G. Vos, *Inorg. Chem.* **1998**, *37*, 5925; l) S. Kar, B. Sarkar, S. Ghumaan, D. Jandananan, J. van Slageren, J. Fiedler, V. G. Puranik, R. B. Sunoj, W. Kaim, G. K. Lahiri, *Chem. Eur. J.* **2005**, *11*, 4901; m) D. Zhang, G.-X. Jin, *Organometallics* **2003**, *22*, 2851; n) S. Scheuermann, T. Kretz, H. Vitze, J. W. Bats, M. Bolte, H. W. Lerner, M. Wagner, *Chem. Eur. J.* **2008**, *14*, 2590; o) G. Nawn, R. McDonald, R. G. Hicks, *Inorg. Chem.* **2013**, *52*, 10912.
- [6] a) J. L. Boyer, T. R. Cundari, N. J. DeYonker, T. B. Rauchfuss, S. R. Wilson, *Inorg. Chem.* **2009**, *48*, 638; b) O. Siri, P. Braunstein, *Chem. Commun.* **2000**, 2223; c) J.-P. Taquet, O. Siri, P. Braunstein, *Inorg. Chem.* **2006**, *45*, 4668; d) C. Tejel, M. A. Ciriano, M. P. del Rio, F. J. van den Bruele, D. G. H. Hetterscheid, N. T. I. Spithas, B. de Bruin, *J. Am. Chem. Soc.* **2008**, *130*, 5844; e) C. Tejel, M. P. del Rio, L. Asensio, F. J. van den Bruele, M. A. Ciriano, N. T. I. Spithas, D. G. H. Hetterscheid, B. de Bruin, *Inorg. Chem.* **2011**, *50*, 7524; f) C. Tejel, L. Asensio, M. P. del Rio, B. de Bruin, J. A. Lopez, M. A. Ciriano, *Angew. Chem. Int. Ed.* **2011**, *50*, 8839; *Angew. Chem.* **2011**, *123*, 9001; g) W. I. Dzik, S. E. Calvo, J. N. H. Reek, M. Lutz, M. A. Ciriano, C. Tejel, D. G. H. Hetterscheid, B. de Bruin, *Organometallics* **2011**, *30*, 372; h) C. Tejel, M. P. del Rio, M. A. Ciriano, E. J. Reiserje, F. Hartl, S. Zalis, D. G. H. Hetterscheid, N. T. I. Spithas, B. de Bruin, *Chem. Eur. J.* **2009**, *15*, 11878; i) C. Tejel, M. A. Ciriano, M. P. del Rio, D. G. H. Hetterscheid, N. T. I. Spithas, J. M. M. Smits, B. de Bruin, *Chem. Eur. J.* **2008**, *14*, 10932; j) C. Tejel, L. Asensio, M. P. del Rio, B. de Bruin, J. A. Lopez, M. A. Ciriano, *Eur. J. Inorg. Chem.* **2012**, 512.
- [7] a) S. Hohloch, P. Braunstein, B. Sarkar, *Eur. J. Inorg. Chem.* **2012**, 546; b) N. Deibel, D. Schweinfurth, S. Hohloch, J. Fiedler, B. Sarkar, *Chem. Commun.* **2012**, 48, 2388; c) N. Deibel, D. Schweinfurth, S. Hohloch, M. Delor, I. V. Sazanovich, M. Towrie, J. A. Weinstein, B. Sarkar, *Inorg. Chem.* **2014**, *53*, 1021.
- [8] a) H. S. Das, F. Weisser, D. Schweinfurth, C.-Y. Su, L. Bogani, J. Fiedler, B. Sarkar, *Chem. Eur. J.* **2010**, *16*, 2977; b) D. Schweinfurth, H. S. Das, F. Weisser, D. Bubrin, B. Sarkar, *Inorg. Chem.* **2011**, *50*, 1150; c) F. Weisser, R. Huebner, D. Schweinfurth, B. Sarkar, *Chem. Eur. J.* **2011**, *17*, 5727; d) M. G. Sommer, D. Schweinfurth, F. Weisser, S. Hohloch, B. Sarkar, *Organometallics* **2013**, *32*, 2069; e) D. Schweinfurth, M. M. Khusniyarov, D. Bubrin, S. Hohloch, C.-Y. Su, B. Sarkar, *Inorg. Chem.* **2013**, *52*, 10332; f) H. S. Das, D. Schweinfurth, J. Fiedler, M. M. Khusniyarov, S. M. Mobin, B. Sarkar, *Chem. Eur. J.* **2014**, *20*, 4334; g) D. Schweinfurth, Y. Reckemmer, S. Hohloch, N. Deibel, I. Peremykin, J. Fiedler, R. Marx, P. Neugebauer, J. van Slageren, B. Sarkar, *Chem. Eur. J.* **2014**, *20*, 3475.
- [9] G. Mazzone, E. Russo, E. Sicilia, *Inorg. Chem.* **2011**, *50*, 10091.
- [10] M. Krejciak, M. Danek, F. Hartl, *J. Electroanal. Chem.* **1991**, *317*, 179.

Received: April 27, 2014

Published online on September 22, 2014